2014

Compressible dynamic stall control using high momentum microjets

Beahan, James J.

Exp Fluids (2014) 55:1813
http://hdl.handle.net/10945/50214

Exp Fluids (2014) 55:1813
DOI 10.1007/s00348-014-1813-6

RESEARCH ARTICLE

Compressible dynamic stall control using high momentum microjets

James J. Beahan · Chiang Shih · Anjaneyulu Krothapalli · Rajan Kumar · Muguru S. Chandrasekhara

Received: 29 January 2014 / Revised: 1 August 2014 / Accepted: 12 August 2014 / Published online: 23 August 2014

Abstract Control of the dynamic stall process of a NACA 0015 airfoil undergoing periodic pitching motion is investigated experimentally at the NASA Ames compressible dynamic stall facility. Multiple microjet nozzles distributed uniformly in the first 12 % chord from the airfoil's leading edge are used for the dynamic stall control. Point diffraction interferometry technique is used to characterize the control effectiveness, both qualitatively and quantitatively. The microjet control has been found to be very effective in suppressing both the emergence of the dynamic stall vortex and the associated massive flow separation at the entire operating range of angles of attack. At the high Mach number ($M = 0.4$), the use of microjets appears to eliminate the shock structures that are responsible for triggering the shock-induced separation, establishing the fact that the use of microjets is effective in controlling dynamic stall with a strong compressibility effect. In general, microjet control has an overall positive effect in terms of maintaining leading edge suction pressure and preventing flow separation.

1 Introduction

Next generation flight vehicles, both fixed and rotary wing, are expected to perform post-stall maneuvers to achieve tactical advantages. This can result in flight at high angles of attack, and knowledge of the nonlinear aerodynamics including strong viscous effects leading to flow separation become very important in the design. Rotary wing aircraft particularly experience a complex aerodynamic phenomenon at high angles of incidence, well known as dynamic stall, involving large variations in lift and strong pitching moments (Ham and Garelick 1968; Carr 1988; Lorber et al. 1992; Chandarasekhara et al. 1993, 1994, 1995, 1998; Shih et al. 1995; Kumar 2004; Bousman 2000; Sahin et al. 2003). McCroskey and Fisher (1972) demonstrated the role of vortices in dynamic stall phenomenon.

1.1 Dynamic stall mechanism

As illustrated in Fig. 1, dynamic stall involves an initial increase in lift (beyond static stall, $C_{l\max}$) due to airfoil pitch-up, formation and growth of a vortex near the leading edge, followed by vortex shedding and gross flow separation on the suction side of the airfoil associated with a rapid loss of lift. The dynamic stall vortex initiated near the leading edge slowly travels toward the trailing edge at a speed that is usually a fraction of the freestream velocity U_∞, providing a characteristic travel time scale of $2\pi/\omega = \pi c/kU_\infty$, where $\omega = 2\pi f$ is the radian frequency of oscillation, c is the airfoil chord length, and k is the reduced pitch frequency (typically in the range of 0.025–0.2).

The dynamic stall process on a blade is initiated by the unsteady boundary layer separation near the airfoil's leading edge. During a rapid pitch-up motion, vorticity production is greatly enhanced by the presence of a favorable pressure gradient at the leading edge. At the same time, vorticity accumulates locally due to the slowdown of downstream convection process caused by an

J. J. Beahan · C. Shih · A. Krothapalli · R. Kumar (✉)
Department of Mechanical Engineering, FAMU-FSU College of Engineering, Florida State University, Tallahassee, FL 32310, USA
e-mail: rkumar@fsu.edu

M. S. Chandrasekhara
Department of Mechanical and Aerospace Engineering, Naval Postgraduate School, Monterey, CA 93043, USA

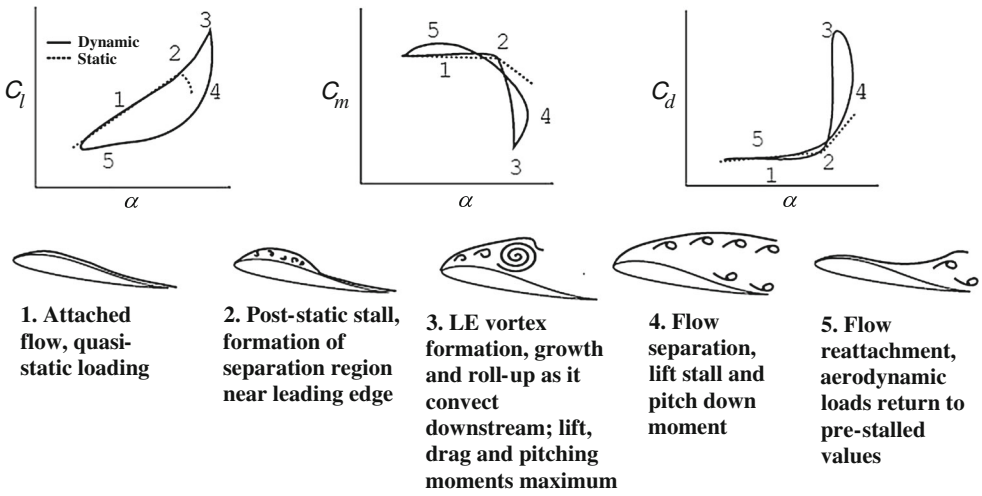

Fig. 1 Dynamic stall mechanisms on an oscillating airfoil (Carr 1988)

adverse pressure gradient and a local boundary layer flow reversal further downstream. The accumulation process is eventually interrupted by a sudden emergence of unsteady flow separation and the subsequent eruption of the accumulated vorticity into the outer flow. Consequently, it initiates a sequence of spontaneous events such as local viscous/inviscid boundary-layer interaction, formation and convection of large energetic vortices and, finally the "stall" and all associated adverse effects. Thus, in order to control the dynamic stall process, a better physical understanding of the unsteady boundary layer separation is necessary.

A detailed theoretical description of the unsteady separation process was first made by Van Dommelen and Shen (1980) using an innovative Lagrangian approach. In short, the process is initiated by a local flow reversal as the result of the adverse pressure gradient. The fastest reversing particles quickly collide with the slower moving particles ahead of them. This results in a local eruption of the particles away from the wall and initiates the separation process. Unlike the traditional shear layer instability mechanism, which selectively amplifies random perturbations in the initial region to develop into organized vortical structures, the deformation triggered by the VDS interaction provides a deterministic perturbation to the local vorticity distribution. After this sudden distortion, the local vorticity arrangement is highly unstable and quickly rolls up into a large dynamic stall vortex (Shih et al. 2003). Once generated, the energetic vortical structure is extremely robust and is difficult, if not impossible, to control. Therefore, any effective control of the dynamic stall process has to be carried out before the formation of the vortex. That is, one has to control the unsteady separation process as described by the VDS model in order to prevent or alleviate the sudden eruption of vorticity from the wall.

1.2 Dynamic stall control methods

There are many ways to implement control on the dynamic stall process to produce the desirable effect. Various methods for control of dynamic stall have been proposed and studied with a reasonable success. These include steady blowing (Carr 1988), suction (Karim and Acharya 1994, Wang 1995) and pulsed blowing (Magill and McManus 1998). In addition, airfoil leading edge geometry modifications have also been investigated, such as leading edge slats (Carr and McAlister 1983), slotted tip (Han and Leishman 2004) and droop (Yu et al. 1995) and dynamically deforming geometries (Chandrasekhara and Ahmed 1993; Chandrasekhara and Carr 1995; Chandrasekhara et al. 1994, 1998; Seifert et al. 1993) and, more recently, Greenblatt and Wygnanski (2001) have shown that periodic zero-net mass-flux excitation through a slot is an effective method for controlling dynamic stall at low speeds ($M \leq 0.12$); however, the strength of the jets is critical if they behave like vortex generators to increase lift or act like spoilers to decrease lift. Lombardi et al. (2012) used plasma actuators to control the dynamic stall at low speeds (10 m/s) and proposed a closed-loop flow control scheme. Nearly all oscillatory methods fix the frequency and amplitude of the actuator perturbation. Relative performance improvements have been studied parametrically by comparing the system response when the controller is "on" to the response when the controller is "off." The full power of feedback control, employing real-time feedback of physically realizable measurements, has not yet been studied. Greenblatt et al. (2001) show that periodic excitation can effectively eliminate the DSV and significantly attenuate dynamic stall over the tested range of Reynolds number and reduced frequencies. The hysteresis in the lift and pitching moment curves are significantly reduced, and the pitching moment excursions are maintained within

acceptable levels. Another key conclusion was that the fluctuations in the aerodynamic coefficients were negligibly small. Recently, Gardner et al. (2014) optimized the use of air jets to control shock-induced dynamic stall on OA209 airfoil. Their results show that jet spacing and supply pressure play an important role in the optimal control of dynamic stall.

In the present study, we demonstrate the implementation of a distributed, multiple microjet control system to provide high-energy perturbations for the compressible dynamic stall control. The microjet control system employed in the present experimental investigation is similar to the system we used successfully in the control of supersonic impinging jets (Alvi et al. 2008; Kumar et al. 2009), separation control on a Stratford ramp (Kumar and Alvi 2006), low-pressure turbine blade (Fernandez et al. 2013) and cavity resonance control (Zhuang et al. 2006). These microjets were driven with higher plenum pressure to achieve a very high momentum. Due to their much smaller size (200–400 μm), the total blowing mass flux from these microjets is very small as compared to the flow being controlled. However, their higher momentum and optimized spacing provide an advantage to achieve the effective flow control. A second advantage of using the microjets is that they can be produced in large quantity and selectively patterned by taking advantage of existing micro-fabrication techniques. Therefore, it is possible to fabricate an assembly of a very large number of microjets with desired spatial distribution for multiple-point control. Finally, micro-fabricated sensors can be packaged with the control unit for multiple-point signal detection and control activation. This makes in situ active flow control possible. This paper clearly demonstrates the potential effectiveness of active flow control using high momentum microjets in suppressing both the emergence of the dynamic stall vortex and the associated flow separation. The effectiveness of control is demonstrated over the range of Mach numbers and angle of attack conditions, particularly eliminating shock-induced separation at high Mach numbers.

2 Experimental setup

2.1 Test facilities

The experiments were conducted at the compressible dynamic stall facility (CDSF) at the NASA Ames Research Center Fluid Mechanics Laboratory in Moffett Field, California. The CDSF is an in-draft wind tunnel with a 25.4 cm × 35.56 cm test section. The CDSF is a facility specifically designed for studying the phenomena of dynamic stall over a range of freestream Mach numbers and reduced frequencies. The facility is equipped with a drive system involving an AC motor, optical encoder and a set of pulleys for generating a sinusoidal variation of airfoil angle of attack. Inside the test section, the airfoil is held between two 2.54 cm thick metal windows using tangs. Optical quality glass inserts in the windows allow light to pass through the test section around the airfoil making direct visualization possible. For a more detailed description of the facility, reference can be made to Chandrasekhara and Ahmed (1993) and Chandrasekhara et al. (1994).

2.2 Test models

To mimic a rotor blade, the test model used was a NACA 0015 airfoil with a chord length (C) of 152.4 mm and span (S) of 248.9 mm. The geometrical details and a picture of the test model are shown in Fig. 2. A total of 424 microjets, with a diameter of 400 μm were placed in a rectangular pattern covering the leading edge, upper nose region and continuing back over the airfoil to 12 % of chord length. Typically, microjets are found to be most effective when placed just upstream of the separation location. The spacing between the microjets was 16 microjet diameters (6.4 mm × 6.4 mm) in zone 1 and zone 3, whereas 12 microjet diameters (4.8 mm × 4.8 mm) in zone 2. This spacing was chosen based on our previous parametric optimization studies (Alvi et al. 2008; Kumar and Alvi 2006; Fernandez et al. 2013) involving flow separation and its control. The microjet interspacing is optimal if the counter rotating pairs of vortices generated by these microjets are fully developed and last longer to enhance the mixing of freestream high momentum fluid with slow moving fluid in the boundary layer.

The microjets were drilled normal to the surface at each location as shown in Fig. 2c. To power the microjets, a plenum cavity (volume ≈ 170 cm^3) was created in a hollowed out nose of the airfoil. The plenum received a compressed air supply via the tangs supporting the airfoil. The pressure inside the plenum cavity was monitored at the extension where the air enters the airfoil outside the testing rig. The microjets' pressure was measured using a Weston Aerospace DPM7885 precision pressure module. The pressure loss between the extension where the pressure is measured during experimentation and the plenum was found experimentally for each microjet setup. The microjets were operated at a plenum pressure between ∼103 and 427 kPa (15 and 62 psia); however, it was typically run at ∼150 kPa (21.7 psia) unless specified otherwise; this microjet plenum pressure was chosen based on our previous experiments (Kumar and Alvi 2006). The total mass injection rate from microjet system operated at this condition was 0.016 kg/s, and the corresponding momentum coefficient (at $M = 0.3$), C_μ was 0.023. C_μ is defined as:

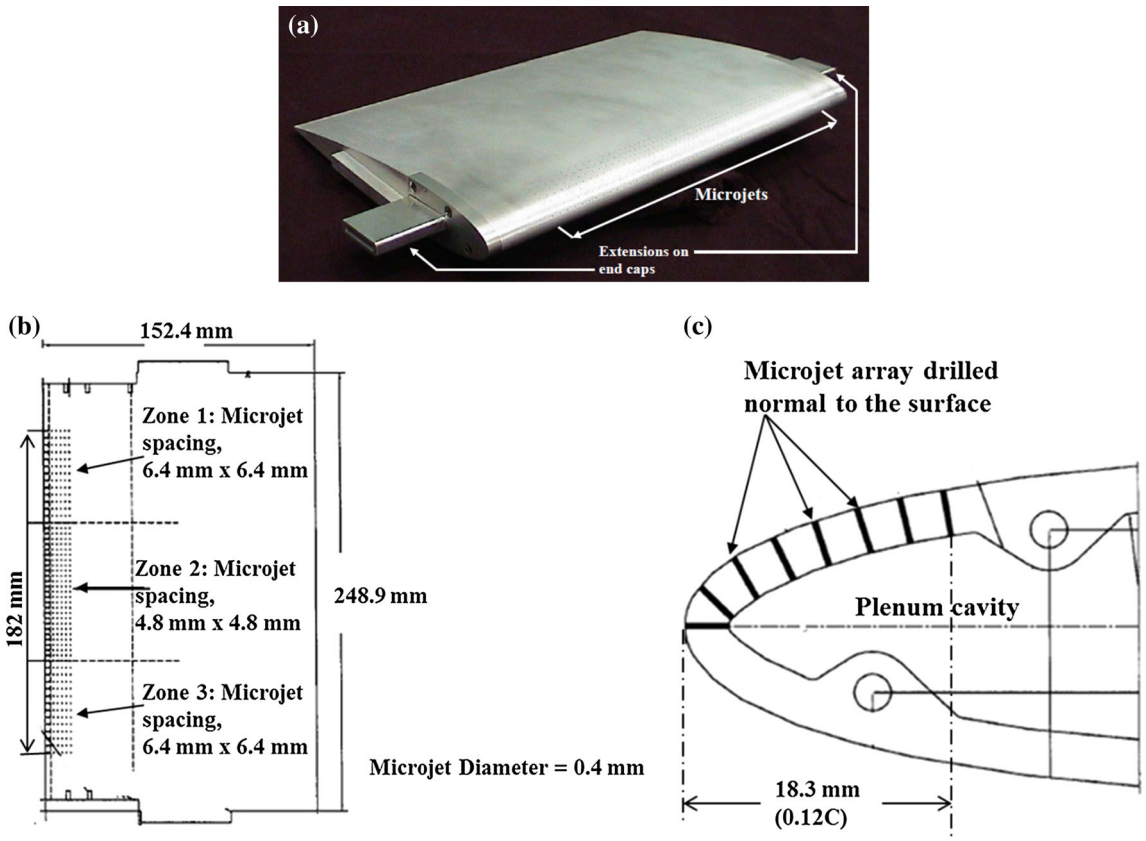

Fig. 2 Geometrical details of NACA 0015 airfoil with microjets. **a** Photograph of the test model, **b** top view of the test model, **c** airfoil leading edge

$$C_\mu = \frac{\dot{m} U_{mj}}{1/2 \rho_\infty U_\infty^2 SC}$$

where $\dot{m}$ is the microjet mass flow rate (measured using an inline mass flow meter), U_{mj} is the microjet velocity at the exit (estimated using isentropic relations based on microjet plenum pressure and tunnel static pressure), ρ_∞ and U_∞ are the freestream density and velocity, respectively. The span and the chord of the airfoil are denoted by S and C, respectively.

2.3 Instrumentation and measurements

For data acquisition purposes, point diffraction interferometry (PDI) was used. PDI (Chandrasekhara and Carr 1995; Chandrasekhara et al. 1994, 1998) is a noninvasive optical technique that measures changes in the index of refraction due to density changes in the compressible flow field. A schematic of the PDI setup is shown in Fig. 3. This technique utilizes the ability of a point discontinuity (a pinhole in this present case) to diffract a portion of incident light into a spherical wave front such that it can function as a point source of light itself. In the present system, a single-pulsed Nd-YAG laser beam of 532 nm wavelength is collimated and expanded through a microscope objective lens and directed through the test section using a high quality, 0.45-m diameter and 3-m focal length parabolic mirror. A second parabolic mirror refocuses the light to the diffraction plate via a modified Z-type Schlieren configuration. The mirrors are located at a distance of 3 m from the test section centerline.

The current PDI plate is a holographic plate that consists of a diffraction pinhole centered in the semi-transparent film plate. A portion of the beam passes through the plate with controlled level of attenuation. On the other hand, the light passing through the center hole creates a spherical diffraction wave that acts as the reference beam for the interferometry effect. A fringe pattern is generated when the reference beam, passing through the center hole, interacts with the attenuated light passed through the other area of the plate. The interference pattern is projected on an ASA 3000 Polaroid film for image recording. Selected Polaroid photographs were digitized at a resolution of 1,200 dpi to allow for accurate image recognition and fringe counting. A detailed description on the fringe processing and data interpretation can be found in Chandrasekhara et al. (1994).

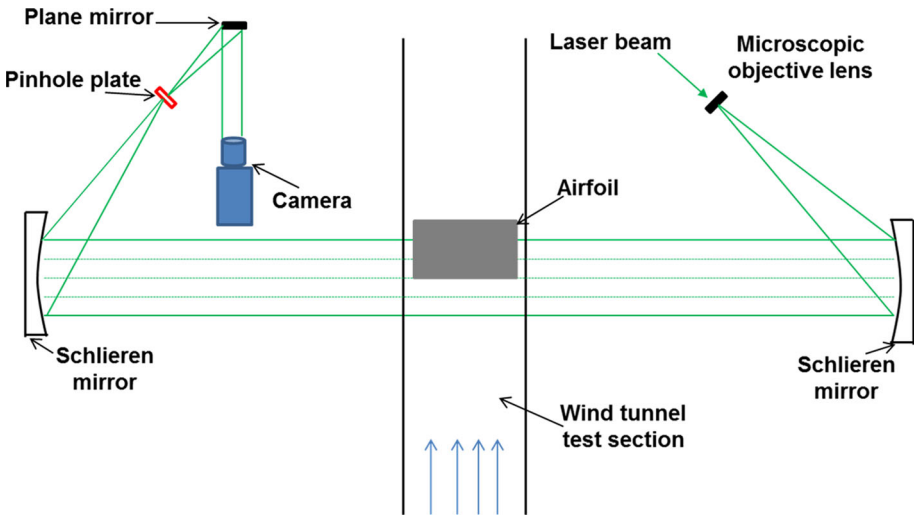

Fig. 3 Point diffraction interferometry setup

2.4 Test conditions

There were three major test parameters for these experiments: Mach number, non-dimensional pitch rate and the airfoil angle of attack. Two flow Mach numbers, $M = 0.3$ and 0.4, were examined; the higher Mach number case corresponded to flow with strong compressibility effects. A combination of high angle of attack ($\alpha \geq 12°$) and relatively higher Mach number condition ($M = 0.4$) resulted in high acceleration of flow near the leading edge and emergence of local shock waves on the upper surface of the airfoil. The test Reynolds number based on airfoil chord was 1.1×10^6 at a Mach number of 0.3 and 1.4×10^6 at a Mach number of 0.4. The velocities were calculated using isentropic flow identities, where stagnation pressure and dynamic pressure were measured in the wind tunnel. The non-dimensional pitch rate was varied between $k = 0.05$ and $k = 0.10$. The angle of attack was varied via following the function:

$$\alpha = 10 + 10\sin(\omega t)$$

2.5 Measurement uncertainties

The accuracy of the measured quantities depends on the individual accuracy of various measuring instruments used and on the flow parameters. The dynamic pitching of the airfoil was accomplished using an AC motor and optical encoder drive. The estimated uncertainties in the data are given below.

$$\Delta M = \pm 0.005 \quad \Delta k = 0.005 \quad \Delta\alpha = 0.05°$$

$$\Delta C_p = \pm 0.1 \quad \Delta C_{p\,\min} = \pm 0.5$$

The uncertainty in the measurement of Mach number depends upon the pressure sensors used to measure the stagnation and static pressure in the wind tunnel. Pressures along the surface are calculated from fringe numbers and tunnel conditions using Gladstone-Dale equation and isentropic flow relations (Carr et al. 1994). The uncertainty in C_p depends on the undetectable fringes under consideration and is one fringe for the flow in general, with up to three fringes near the shock or suction peak. As the total mass flow injection rate for the present experiments was less than 0.03 kg/s, the estimated change in temperature or the density in the boundary layer due to microjet injection is less than 1 %. Due to the changes in back pressure during pitch oscillation cycle, the variation in microjet momentum is estimated to be less than 5 %.

3 Results and discussion

3.1 Interpretation of interferograms

The interferograms obtained from the corresponding flow conditions contain information that is both qualitative (as flow visualization) and quantitative in nature. Using image digitization and fringe-counting scheme, these images can yield many useful quantities such as the surface pressure distributions. In the following, we are going to first address the qualitative observations that provide a better understanding of the flow physics related to the emergence of dynamic stall and then the quantitative results.

Figure 4 is a typical interferogram image taken at the condition of $M = 0.3$, $k = 0.10$, and $\alpha = 18°$. This image exemplifies many important features of the flow dynamics of the airfoil undergoing pitching-up motion. The first prominent feature is the existence of the stagnation region near the leading edge on the lower surface. This region can be identified as where the local fringe circle around and reconnects with the airfoil's surface in the lower left-hand

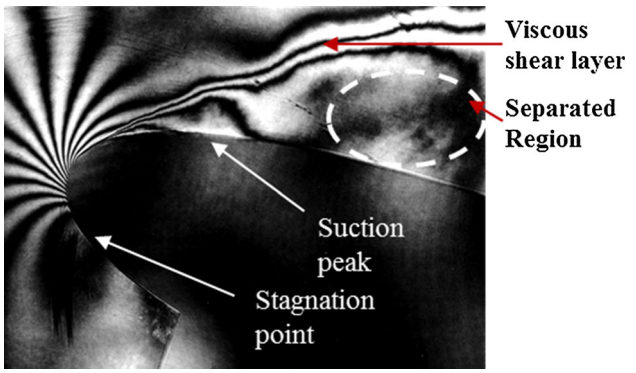

Fig. 4 Point diffraction interferogram, no control, $M = 0.3$, $k = 0.10$, and $\alpha = 18°$

portion of the image. The stagnation point can be identified at the center of this stagnation bubble where the pressure is a local maximum.

Another interesting aspect is the concentration of fringes near the leading edge indicating the existence of a large density (or pressure) gradient due to the rapid acceleration of the flow over the airfoil's nose. These local fringes also form a recirculated pattern as they emerge from the airfoil's surface and circles around to reconnect with the surface again. This pattern is due to the existence of a locally minimum pressure near the airfoil's nose. In this sample image, the peak fringe number counted is 8, which corresponds to a local pressure of 85.9 kPa and a local Mach number of 0.91 (a linear, isentropic relation is used to estimate the local Mach number and it can only be used as a reference.) The rapid acceleration of flow from stagnation to close to sonic condition is responsible for generating the local suction pressure near the airfoil nose, thus the generation of lift. Also notice the existence of a large separation region downstream from the leading edge (marked with dotted ellipse). This condition does not appear in every case but only in cases where massive separation has dominated due to the emergence of the catastrophic stall. Inside the separation region, no obvious fringe pattern can be observed due to the turbulent nature of the flow. A relatively flat pressure distribution is expected within this area.

3.2 Effect of microjet control at $M = 0.3$

Figure 5a–c show three representative interferograms for the case of $M = 0.3$ and $k = 0.1$ without control. This sequence shows the reattachment of the separation region as the airfoil pitches down from high to low angles of attack. The first two images show total flow separation with a detached shear layer away from the airfoil. In Fig. 5b, the appearance of a closed fringe region above the airfoil in the center of picture might be indicative of the release of a vortex from the leading edge.

In Fig. 5c, the separated shear layer seems to reattach back to the surface. The increase of the number of the fringes suggests the increase of suction pressure near the leading edge and the recovery of lift. An interesting observation is the bending of the reattaching fringes when they approach closely to the airfoil surface. They tend to curve upstream and align parallel to the surface. This is due to the non-uniform temperature inside the boundary layer; the fringes (constant density lines) are actually aligned closely with constant temperature lines and not the constant pressure lines. On the other hand, this local fringe bending makes the identification of the edge of the boundary layer easier (Fig. 5c).

Figure 6a–c show corresponding cases with microjet control (with a control pressure of 21.7 psia.). The location of microjet array is shown in Fig. 6a. The microjet streams can be clearly seen in the upper leading edge region. The presence of these jet streams distorts the local fringe patterns, as one would expect from the flowfield of jet in a crossflow. Amazingly, the leading edge flow appears to remain attached at all the angles of attack when the microjet control is turned on. The increase in the number of the interference fringes near the leading edge is indicative of the fact that lower suction pressure is maintained near the nose if the microjet control is used. Qualitatively, one can conclude that the microjet control is extremely effective in eliminating the massive flow separation that was observed in the baseline flow without control.

On the other hand, these images also show that, with control, the viscous boundary layer appears to be thicker (see Fig. 6c as an example) when compared to an attached case without control (Fig. 5c). This is expected since a significant amount of fluid is being displaced away from the boundary layer due to the blowing of the microjet. Also, with control, the fringes align almost normal to the airfoil's surface instead of parallel to it, as is the case without control. This could be explained by realizing that the activation of control has generated many locally separated flow regions behind each of these microjets. These separated regions are highly turbulent with strong mixing characteristics, yet they are small enough to not trigger a massive separation. The culmination of these small-scale separated regions can lead to the thickening of the boundary layer. Microjets are known to produce streamwise vortices (Alvi et al. 2008; Zhuang et al. 2006) and increase the mixing of high momentum outer flow with the less energetic boundary layer flow. The new thickened boundary layer is more energetic and of high momentum than the uncontrolled boundary layer. Also, one would expect that the temperature is reasonably uniform inside

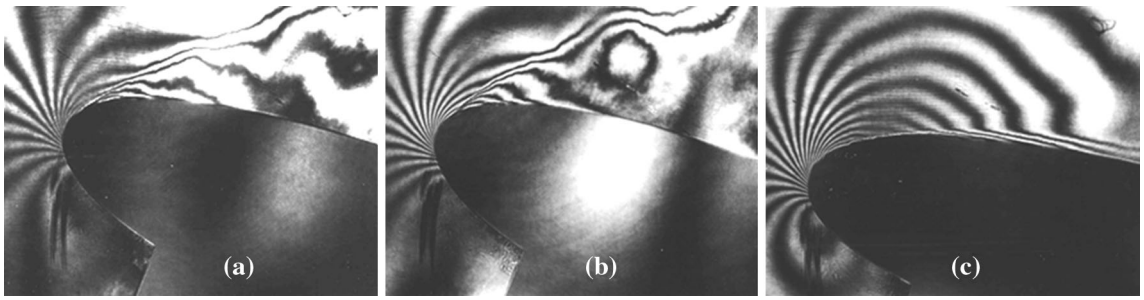

Fig. 5 Flow sequence of a pitching airfoil, $M = 0.3$, $k = 0.10$, without control. **a** $\alpha = 19.9°$ upward, **b** $\alpha = 19.0°$ downward, **c** $\alpha = 13.1°$ downward

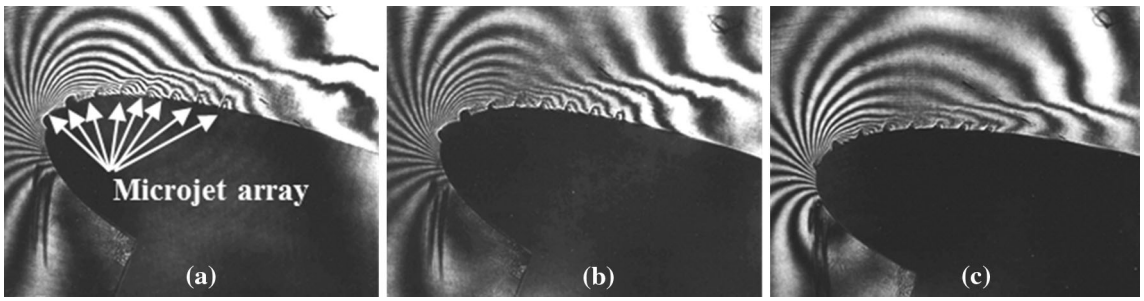

Fig. 6 Flow sequence of a pitching airfoil, $M = 0.3$, $k = 0.10$, with control (control pressure 21.7 psia, $C_\mu = 0.023$). **a** $\alpha = 19.9°$ upward, **b** $\alpha = 19.0°$ downward, **c** $\alpha = 13.1°$ downward

the thickened layer accompanied with a more uniform density profile. Therefore, constant density lines (fringes) are expected to coincide with constant pressure lines, which are aligned normal to the airfoil's surface according to the boundary layer theory. On the other hand, a sharp discontinuity of the slope of the local fringe can be seen between the thick inner layer and the outer flow. This suggests the existence of another thin outer layer separating the external flow stream from the inner viscous layer. The seemingly streamwise alignment of fringes inside this outer layer suggests the existence of a substantial vorticity gradient across the layer, the characteristic of the presence of a strong shear. It is reasonable to believe that this thin outer layer originates from the leading edge vorticity layer as it is displaced by the outward blowing microjets. Being moved away from the surface, this vorticity layer can now convect effectively downstream to prevent the significant local accumulation that might lead to the subsequent emergence of dynamic stall. The effective release of vorticity by displacing it away from the surface appears to be one of the major mechanisms why the microjet control scheme works.

The results at a reduced pitch frequency $k = 0.05$ for the baseline flow without control and with microjet control are presented in Figs. 7 and 8, respectively. This sequence shows the baseline case (Fig. 7) developing from no stall, attached flow below 12° through stall with flow separation near 15.9° to the top of rotation at 20° with detached shear layer and highly separated flow. In contrast, all three of these cases with control (Fig. 8) clearly exhibits completely attached flow with no separation bubble and thus have not stalled. Further, all the features discussed for the $k = 0.10$ case (Figs. 5, 6) are present at $k = 0.05$ and nearly identical including the viscous boundary layer and its deflection with control activated. These findings are more impressive than for the previous case due to the fact that dynamic stall occurs at a lower angle of attack and the control scheme exhibits an equally dominant effect in mitigating dynamic stall.

3.3 Effect of microjet control at $M = 0.4$

Upon increasing the freestream Mach number to 0.4, a portion of the flow over the airfoil reaches supersonic speeds, as exemplified by the presence of shocks in Fig. 9a. These shocks only exist through a small range of angles of attack from $\alpha = 12.5°$ to $\alpha = 14.6°$. However, they play a significant role in the initiation and progress of the dynamic stall. Due to the presence of an even more severe adverse pressure gradient across a shock, the local boundary layer is more prone to separation and a loss of lift. Therefore, the problem of dynamic stall becomes even severe at higher Mach numbers.

When the microjets are activated, these shocks disappear as shown in Fig. 9b. Microjet control seems to have

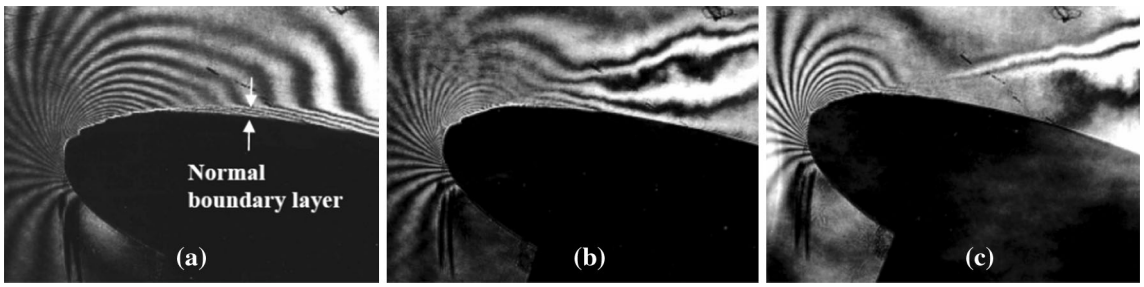

Fig. 7 Flow sequence of a pitching airfoil, $M = 0.3$, $k = 0.05$, without control. **a** $\alpha = 11.5°$ upward, **b** $\alpha = 15.9°$ upward, **c** $\alpha = 20°$

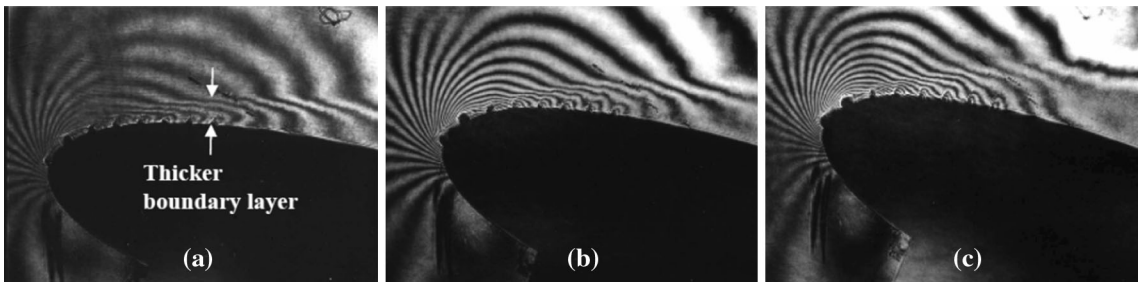

Fig. 8 Flow sequence of a pitching airfoil, $M = 0.3$, $k = 0.05$, (control pressure 21.7 psia, $C_\mu = 0.023$). **a** $\alpha = 11.5°$ upward, **b** $\alpha = 15.9°$ upward, **c** $\alpha = 20°$

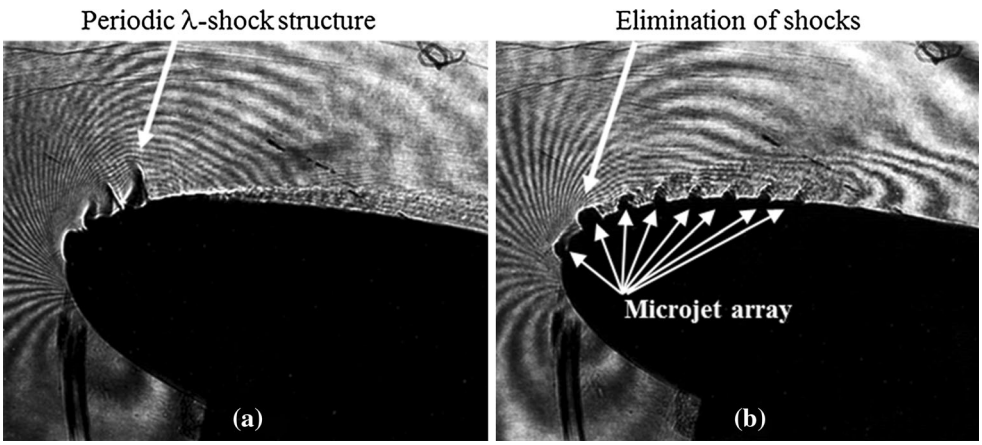

Fig. 9 Effect of microjet control on dynamic stall, $M = 0.4$, $k = 0.05$, $\alpha = 12.5°$, **a** no control, **b** with control $C_\mu = 0.021$

balanced the pressure boundary in the shock region and equalized the pressure across the shock foot. With control, the boundary layer has been thickened significantly similar to $M = 0.3$ cases. Consequently, the dynamic stall has been eliminated or significantly delayed as shown by the following three flow sequences (Figs. 10, 11). We would like to point out that, some (ghost) shadows appear in some of the images shown (mainly in the two lower angle cases) but these do not affect the interpreted results. The appearance of this background noise is the result of having two pinholes placed too close together. The emergence of a very large vortex-like structure is typical of shock-induced separation (Fig. 10a). On the other hand, no vortex or massive separation can be observed if control is used (Fig. 11). These results once again prove the efficacy of microjet-based control in eliminating compressible dynamic stall.

3.4 Pressure distribution on the airfoil surface

In order to obtain quantitative pressure distribution data, selected images were digitized as described in the experimental setup section. The coordinates where the fringes merge with the airfoil's surface and the corresponding fringe numbers were both recorded. If a boundary layer was clearly discernible, the intersection of the fringe and the outer edge of the boundary layer was used instead. Using the processed data, it was possible to calculate the

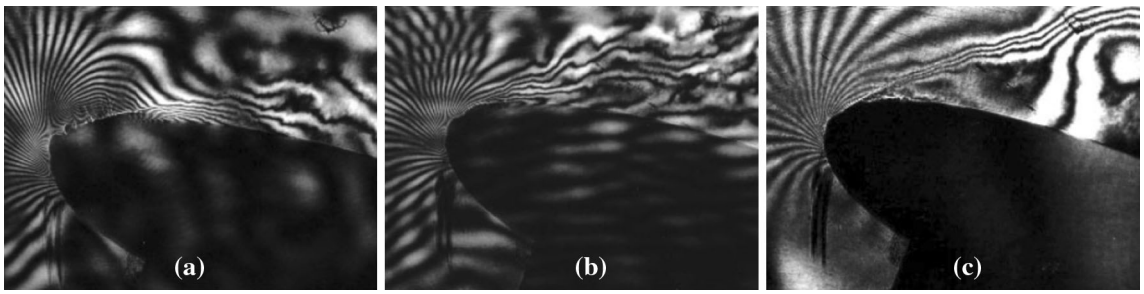

Fig. 10 Flow sequence of a pitching airfoil, $M = 0.4$, $k = 0.05$, without control. **a** $\alpha = 12.9°$ upward, **b** $\alpha = 18°$ upward, **c** $\alpha = 20°$

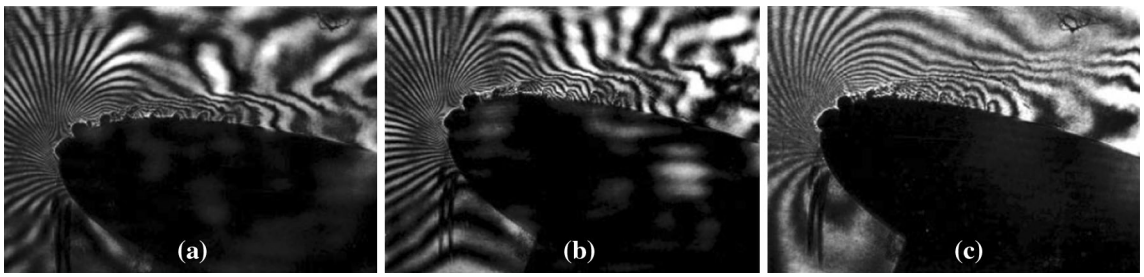

Fig. 11 Flow sequence of a pitching airfoil, $M = 0.4$, $k = 0.05$, with control ($C_\mu = 0.021$). **a** $\alpha = 12.9°$ upward, **b** $\alpha = 18°$ upward, **c** $\alpha = 20°$

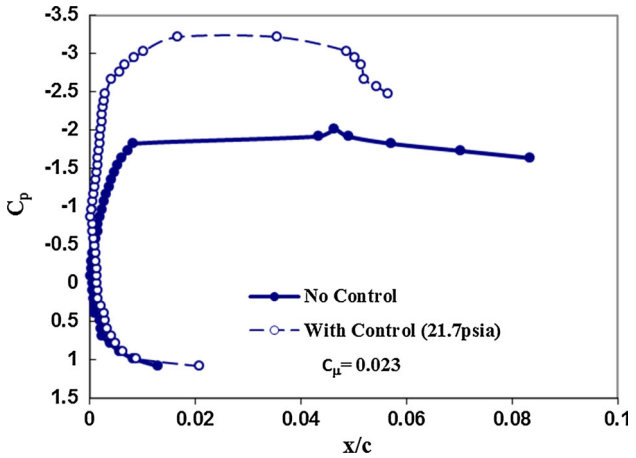

Fig. 12 Pressure distribution on leading edge of airfoil, $M = 0.3$, $k = 0.10$, $\alpha = 16.5°$ pitching downward

pressure distribution in terms of coefficient of pressure (C_p) as a function of chord-wise location (x/c). C_p is defined as:

$$C_p = \frac{p - p_\infty}{1/2 \gamma p_\infty M_\infty^2}$$

where p is the local surface pressure calculated from fringe numbers and tunnel conditions (free stream static pressure p_∞ and Mach number M_∞) using Gladstone-Dale equation and isentropic flow relations (Carr et al. 1994).

Figure 12 shows two representative pressure distributions near the leading edge of the airfoil with and without control. The solid symbols present the distribution with no control, while the open symbols follow the distribution with microjet control. In case of baseline flow without control, the suction pressure does not fall below $C_p = -2.0$ and there is a large region where the pressure is relatively flat ($x/c = 0.01$–0.08), an indication of separated flow. These observations are very similar to those reported by Carr et al. (1994) and Chandrasekhara et al. (1998) using PDI technique on NACA 0012 airfoil. When the microjet control was turned on, the suction pressure re-established by reaching to a much lower value of $C_p = -3.2$, indicating that the region is dominated by a locally attached and accelerating flow.

Another measure of the control effectiveness can be represented by determining the minimum pressure coefficient on the upper airfoil's surface. The corresponding variations of the minimum pressure coefficients with and without control as a function of airfoil angle of attack are presented in Fig. 13. Without control (solid symbols), the minimum pressure initially increases at a relatively constant rate (from an angle of 13° to 16°) and it reaches a lower pressure ($C_p = -5.0$) as the airfoil approaches stall. At this instant, the emergence of a dynamic stall vortex actually induces a low suction pressure near the leading edge to sustain a higher lift. However, as soon as the vortex detaches from the airfoil's nose, this negative pressure peak drops off quickly when massive separation emerges and the airfoil approaches deep stall regime ($\alpha > 16°$). The lowest negative pressure ($C_p = <-2.0$) appears close to when the airfoil reaches to its maximum angle of attack (20°). The

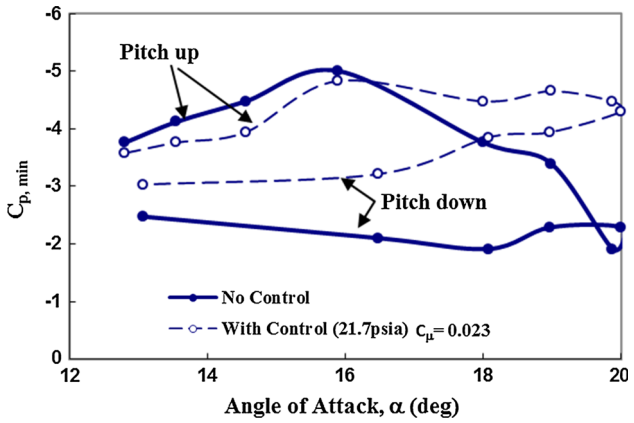

Fig. 13 Peak suction pressure coefficient as a function of angle of attack, $M = 0.3$, $k = 0.10$, with and without control

recovery of the suction peak is slow. As the airfoil pitches down it reaches a value of approximately $C_p = -2.5$ at an angle of attack of 13°. The large difference of the peak suction before and after the stall indicates that the wing is undergoing a very substantial load fluctuation.

Figure 13 clearly shows the effect that the microjets have on the peak suction pressure. Initially, the peak suction pressure is lower when the control is turned on as expected. The timely release of vorticity through outward blowing means there is an overall reduction of the bounded circulation, which is responsible for the generation of the airfoil's lift. Before reaching the stall angle, the lift curve with control, while at a slightly lower value compared to that without control, increases at about the same rate as the no control case. However, instead of dropping off to lose the suction the controlled wing can maintain its maximum suction pressure for an extended range of angles. At the maximum angle of attack, the peak value of $C_p = -4.3$ is about double that of the corresponding no control case ($C_p = -2.2$). There is no significant drop off with control during pitch-up motion even beyond the stall angle of attack (from $C_p = -4.8$ to $C_p = -4.3$). The much smaller hysteresis loop of the suction peak pressure means a more stable flow behavior with microjet control. Similar observations were made by Greenblatt and Wygnanski 2001 for dynamic stall control using periodic excitations at the leading edge. Although not directly relating to the overall lift, the cyclic history of the peak suction pressure suggests that the averaged lift should increase with microjet control. These observations are consistent for the $k = 0.05$ case as well as the cases at $M = 0.4$. The present results clearly show that microjets are potentially an effective means to control compressible dynamic stall behavior.

4 Conclusion

In summary, the microjet control has been shown to be very effective in controlling the dynamic stall process by the use of the PDI technique, both qualitatively and quantitatively. It is speculated that the emergence of a two-layer structure due to microjet blowing is responsible for the control effectiveness. An outer layer effectively convects vorticity away from the leading edge region to avoid local accumulation of vorticity into the dynamic stall vortex. The merging of separated flow pockets behind these microjets forms a thicker inner layer with high mixing characteristics, allowing the boundary layer flow to withstand the emergence of a locally adverse pressure gradient. Microjet control eliminated the λ-shock structures present in the baseline flow at $M = 0.4$ on the suction side near the leading edge of the airfoil. The combination of these effects enables the airfoil to pitch to higher angles of attack without the generation of the dynamic stall vortex and the subsequent massive flow separation. Consequently, suction peak pressure at the leading edge can be maintained for the entire operating range of angles of attack with a more stable flow behavior. Additionally, by stabilizing the flow, it can be used to reduce fluttering noise and the associated flow-induced vibrations. In future, a comprehensive study involving particle image velocimetry and a six-component strain gage balance will be carried out to investigate the effect of microjet control on the compressible dynamic stall. In addition, the use of unsteady microjets capable of operating at a frequency of interest will also be exploited for compressible dynamic stall control.

Acknowledgments This work was supported by a grant from NASA Ames, monitored by Dr. G. Yumauchi; we are grateful for this support. We also thank additional support and technical advices provided by Dr. C. Tung of US Army Aero flight dynamics Division and Dr. J. C. Ross and Dr. R. D. Mehta for allowing the use of the FML CDSF.

References

Alvi FS, Lou H, Shih C, Kumar R (2008) Experimental study of physical mechanisms in the control of supersonic impinging jets using microjets. J Fluid Mech 613:55–83

Bousman WG (2000) Airfoil dynamic stall and rotorcraft maneuverability, NASA/TM-2000-209601

Carr LW (1988) Progress in analysis and prediction of dynamic stall. J Aircr 25:1–25

Carr LW, McAlister KW (1983) The effects of leading edge slat on the dynamic stall of an oscillating airfoil, AIAA Paper 85-2533

Carr LW, Chandrasekhara MS, Brock N (1994) A quantitative study of unsteady compressible flow on an oscillating airfoil. J Aircr 31(4):892–898

Chandrasekhara MS, Ahmed S (1993) Velocity and vorticity distributions over an oscillating airfoil under compressible dynamic stall. AIAA J 31:6

Chandrasekhara MS, Carr LW (1995) Compressibility effects on dynamic stall of oscillating airfoils. AGARD-CP-552, pp. 3.1–3.15

Chandrasekhara MS, Carr LW, Wilder MC (1994) Interferometric investigations of compressible dynamic stall over a transiently pitching airfoil. AIAA J 32:3

Chandrasekhara M, Wilder M, Carr L (1998) Competing mechanisms of compressible dynamic Stall. AIAA J 36:387–393

Fernandez E, Alvi FS, Kumar R (2013) Separation control on a low-pressure turbine blade using microjets. J Propul Power 29:867–881

Gardner AD, Richter K, Mai H, Neuhaus D (2014) Experimental investigation of air jets to control shock-induced dynamic stall. J Am Helicopter Soc 59(2):1–11

Greenblatt D, Wygnanski I (2001) Dynamic stall control by periodic excitation, part 1: NACA 0015 parametric study. J Aircr 38:430–438

Greenblatt D, Nishri B, Darabi A, Wygnanski I (2001) Dynamic stall control by periodic excitation, part 2: mechanisms. J Aircr 38(3):439–447

Ham ND, Garelick MS (1968) Dynamic stall considerations in helicopter rotors. J Am Helicopter Soc 13(2):49–55

Han Y, Leishman J (2004) Investigation of Helicopter Rotor-Blade-Tip-Vortex Alleviation Using a Slotted Tip. AIAA Journal 42:524–535

Karim MA, Acharya M (1994) Suppression of dynamic-stall vortices over pitching airfoils by leading-edge suction. AIAA J 32:1647–1655

Kumar R (2004) Dynamic stall behavior on a pitch oscillating airfoil/wing. NAL-PD-NT-3230

Kumar V, Alvi FS (2006) Use of high-speed microjets for active separation control. AIAA J 44(2):273–281

Kumar R, Lazic S, Alvi FS (2009) Control of high-temperature supersonic impinging jets using microjets. AIAA J 47(12):2800–2811

Lombardi AJ, Bowles PO, Corke TC (2012) Closed-loop dynamic stall control using a plasma actuator. In: 50th AIAA aerospace sciences meeting including the new horizons forum and aerospace exposition, 09–12 January 2012, Nashville, Tennessee

Lorber PF, Carta FO, Covino AF (1992) An oscillating three-dimensional wing experiment: compressibility, sweep, rate, and geometry effects on unsteady separation and dynamic stall. United Technologies Research Center, ReportR92-958325-6, East Hartford, Connecticut

Magill JC, McManus KR (1998) Control of dynamic stall using pulsed vortex generator jets. AIAA-98-0675

McCroskey WJ, Fisher RK (1972) Detailed aerodynamic measurements on a model rotor in the blade stall regime. J Am Helicopter Soc 17(1):20–30

Sahin M, Sankar LN, Chandrasekhara MS, Tung C (2003) Dynamic stall alleviation using a deformable leading edge concept—a numerical study. J Aircraft 40(1):77–85

Seifert A, Bachar T, Shepshelovish M, Wygnanski I (1993) Oscillatory blowing: a tool to delay boundary-layer separation. AIAA J 11:2052–2060

Shih C, Lourenco LM, Krothapalli A (1995) Investigation of flow at leading and trailing edges of pitching-up airfoil. AIAA J 33(8):1369–1376

Shih C, Beahn J, Krothapalli A, Chandrasekhara MS (2003) Control of compressible dynamic stall using microjets. FEDSM2003-45627

Van Dommelen L, Shen SF (1980) The spontaneous generation of the singularity in a separating laminar boundary layer. J Comput Phys 38:125–140

Wang SC (1995) Control of dynamic stall, PhD Dissertation, Mechanical Engineering Department, Florida State University

Yu YH, Lee S, McAlister KW, Tung C, Wang CM (1995) Dynamic stall control for advanced rotorcraft application. AIAA J 33(2):289–295

Zhuang N, Alvi FS, Alkilsar M, Shih C (2006) Aeroacoustic properties of supersonic cavity flows and their control. AIAA J 44(9):2118–2128